JOURNAL OF SPACECRAFT AND ROCKETS
Vol. 30, No. 4, July–August 1993

Low-to-High Altitude Predictions of Three-Dimensional Ablative Re-Entry Flowfields

Bilal A. Bhutta* and Clark H. Lewis†
VRA, Inc., Blacksburg, Virginia 24063

To analyze the coupled effects of ablation and transition/turbulence on the flowfield and aerodynamic forces and moments, a new three-dimensional coupled-chemistry nonequilibrium parabolized Navier-Stokes scheme is developed to predict low-to-high altitude laminar/transitional/turbulent flows over sphere-cone configurations with ablative Teflon surfaces at small angles of attack. The species conservation equations are solved using a two-step approach, and the Teflon surface-ablation rate is predicted using a quasisteady ablation that is coupled with the flowfield solution which includes a detailed representation of the Teflon-ablation process and includes density variations of Teflon. Mach 20 flow over a 6-deg sphere-cone configuration is studied at 50 and 125 kft under 0- and 0.5-deg angles of attack. The results obtained indicate that, as the transition front moves upstream over the body, the vehicle's center of pressure first increases by several percent, reaches a maximum, and then decreases as the flow becomes fully turbulent. Results also suggest that additional considerations such as asymmetric transition front and transition lengths can further enhance these effects on the center-of-pressure location.

Nomenclature

CA	= axial-force coefficient
C_i	= mass fraction of the ith species
CM	= pitching moment coefficient (with respect to the nose)
CN	= normal-force coefficient
Cp	= specific heat at constant pressure
D_{ij}	= diffusion coefficient for the ith species with respect to the jth species
E_i	= mass fraction of the ith element
h	= static enthalpy of the mixture
J	= determinant of the transformation Jacobian
k	= thermal conductivity
L	= total body length, ft
Le	= binary Lewis number, $\rho C_p D_{ii}/k$
M	= Mach number
$MDOT$	= $\dot{m}$
$\bar{m}$	= mixture molecular weight
$\dot{m}$	= surface ablation rate, $(\rho w)_w/\rho_\infty V_\infty$
m_{njk}	= $\xi_{n,j}\xi_{n,k}$, where $n = 2$ or 3
NE	= total number of elements
NM	= total number of group 1 species
NS	= total number of chemical species
$PINF$	= freestream pressure, p_∞, lbf/ft^2
Pr	= Prandtl number
p	= static pressure, lbf/ft^2
Q_c	= conduction component of the heat transfer rate, Btu/ft^2-s
Q_d	= diffusion component of the heat transfer rate, Btu/ft^2-s
R	= radial distance from body axis, ft
R_b	= local body radius, ft
Re	= Reynolds number, $(\rho VRn)/\mu$
RN, Rn	= nose radius, ft
T	= static temperature, °R
$TINF$	= freestream static temperature, T_∞, °R
U_j	= contravariant velocities, $u_k\xi_{k,x_j}$, 1/s
u	= x component of mass-averaged velocity, ft/s
u_j	= u, v, and w for $j = 1$, 2, and 3, ft/s
V	= total mass-averaged velocity, ft/s
v	= y component of mass-averaged velocity, ft/s
v_w	= wall injection velocity, ft/s
w	= z component of mass-averaged velocity, ft/s
X, x	= coordinate along body axis, ft
XCP	= axial location of the center of pressure, ft
x_j	= x, y, and z for $j = 1$, 2, and 3, ft
Y	= y coordinate, ft
Z	= z coordinate, ft
α	= angle of attack, deg
ϵ	= M_∞/Re_∞
μ	= viscosity, lbf-s/ft^2
ξ_1	= marching or streamwise coordinate
ξ_2	= coordinate measured from the body to the outer bow shock
ξ_3	= crossflow coordinate
ρ	= mixture density, slug/ft^3
$\dot{\omega}_i$	= production rate of the ith species

Superscripts

EQ	= equilibrium conditions
n	= index for iteration
T	= vector or matrix transpose
-	= mixture property

Subscripts

a	= amorphous Teflon
i	= ith chemical species or in-depth conditions
j, k, l	= indicial notation representing 1, 2, and 3
s	= shock quantity or solid Teflon
w	= wall quantity
$'$	= partial derivative
∞	= freestream

Received Oct. 22, 1992; revision received Jan. 22, 1993; accepted for publication Jan. 25, 1993.

*Vice President. Senior Member AIAA.
†President. Associate Fellow AIAA.

Introduction

RECENTLY we developed and presented a new axisymmetric nonequilibrium coupled-chemistry parabolized Navier-Stokes (PNS) scheme capable of treating the entire range of equilibrium to nonequilibrium to frozen flow conditions[1] and demonstrated it by treating clean air (nonablative) re-entry flows from sea level to 250 kft. We also developed a

Table 1 Freestream conditions for cases 1-3

Quantity	Case 1	Cases 2 and 3
Mach number	20	20
Altitude, kft	50	125
Pressure, lbf/ft^2	244.85	7.76
Temperature, °R	389.1	442.7
Wall temperature, °R	1800	1800
Angle of attack, deg	0	0, 0.5

new quasisteady ablation model for Teflon which was locally coupled to the flowfield solution to predict the associated surface-ablation rates.[1] Moreover, in addition to being axisymmetric, the flowfields considered were limited to laminar flows.

The results of our earlier axisymmetric study[1] were very encouraging and motivated the extension to study low-altitude nonequilibrium (finite rate) turbulent re-entry flows at small angles of attack with Teflon surface ablation. The major objective behind this extension was to study the coupled effects of ablation and transition/turbulence on the flowfield and aerodynamic forces and moments.

In this paper we present the approach used and the results from our three-dimensional angle-of-attack studies. In general, these three-dimensional results are very encouraging and interesting and clearly indicate that, when the effects are coupled together, transition/turbulence and ablation can have noticeable effects not only on the flowfield and plasma levels but also on the vehicle center of pressure. In fact, the results show that as the transition front moves upstream over the body, the vehicle center of pressure first increases by several percent, reaches a maximum, and then decreases as the flow becomes fully turbulent. Some simplifying assumptions (symmetric transition front, instantaneous transition, constant altitude and freestream conditions, constant angle of attack, etc.) were made in this study to reduce ambiguity. In reality, the transition front is asymmetric, the flow is transitional with potentially different transition lengths on the windward and leeward sides, and the vehicle is constantly descending in altitude. All of these real effects can introduce other significant asymmetries in the flowfield and, thus, may lead to an even greater variation in the aerodynamic center of pressure. The impact of vehicle length was also considered in this study. The present approach, although limited to small angles of attack, represents a realistic three-dimensional treatment of the combined flowfield and ablation effects.

The baseline PNS scheme used in this study has been developed by us over the past several years[1-13] and uses a uniquely accurate solution scheme (free of any sublayer-type approximation[11,12]) along with an iterative numerical approach based on a pseudounsteady technique to the final steady-state solution. It uses a new nonequilibrium coupled-chemistry solution scheme which is also stable in the equilibrium (infinite reaction rate) and frozen (zero reaction rate) limits.[1] Typically, for equilibrium or near-equilibrium flows, the species conservation equations become numerically stiff and must be solved in a mutually coupled manner.[14] Different workers have used different forms of this coupling[15,17]; however, we have shown that in the afterbody region only a mutual coupling of the species is necessary and sufficient.

In our earlier laminar axisymmetric study,[1] we developed and investigated three types of numerical solution schemes for solving the nonequilibrium species conservation equations: 1) a strongly implicit scheme, 2) a two-step scheme, and 3) a diagonalized scheme. Several test cases (mostly laminar nonablative flows) were done to demonstrate that the new two-step solution approach for solving the species conservation equations was a very attractive approach because it not only avoids the numerical stiffness problem, but it is also the most efficient in terms of computational speed.[1] In this study we have used this two-step solution scheme for studying three-dimensional turbulent re-entry flows with ablating Teflon surfaces.

Teflon-Air Chemical Model

Teflon (C_2F_4) is a fluorocarbon polymer compound most commonly used as a low-temperature ablator for heat-shield applications and for the purpose of shock-layer electron quenching. The present Teflon-air chemical model is based on the data used by Bhutta and Lewis,[1,6] Bhutta et al.,[7] and Blottner et al.[18] In this chemical model, Na and Na^+ were included to simulate the effects of alkali metal contamination on the ablation products. For most of this study the sodium contamination at the wall was assumed to be 150 ppm; however, contamination levels of 50 and 250 ppm were also tested to see their impact on the predicted peak electron number densities.

The Teflon-air chemical model used in this study has been discussed in detail by Bhutta and Lewis.[1] Briefly stated, the overall Teflon-air chemical system used consists of 23 species (O, O_2, N, N_2, NO, C, C_2, C_3, CO, CO_2, Na, F, F_2, CF_2, CF_4, COF_2, C_2F_4, NO^+, O^-, O_2^-, Na^+, F^-, and e^-) and 36 gas-phase reactions.[1] The associated thermodynamic and transport properties of these 23 Teflon-air species are also described in Ref. 1. The thermal conductivity of the individual species is calculated from the Eucken semiempirical formula, and the viscosity and thermal conductivity of the mixture are calculated using Wilke's semiempirical relations.[1] The diffusion model used in the present study was limited to binary diffusion, and the binary diffusion coefficients were estimated using a constant binary Lewis number of 1.4.[1]

Solution Scheme

The coordinate system used for the present three-dimensional PNS scheme is a general curvilinear coordinate system (ξ_1, ξ_2, ξ_3). The ξ_1 coordinate is along the body and is also the marching direction, the axis-normal ξ_2 coordinate stretches from the body to the outer bow shock, and the ξ_3 coordinate is the circumferential coordinate measured from the windward pitch plane to the leeward pitch plane. Also, a body-fixed orthogonal (Cartesian) coordinate system is chosen such that the origin of the Cartesian coordinate system is at the tip of the blunt nose, and the x axis is aligned with the axis of the body.

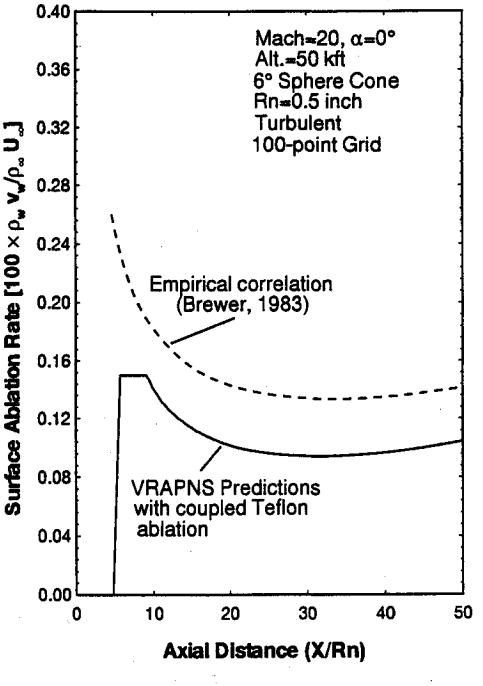

Fig. 1 Comparison of predicted ablation rate at 50 kft.

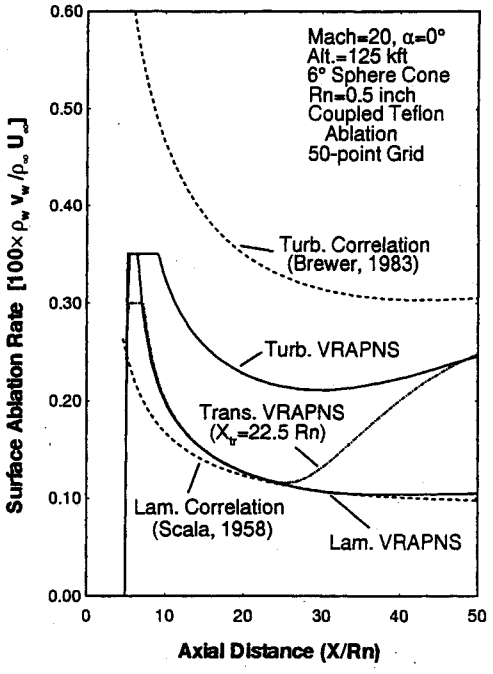

Fig. 2 Comparison of predicted ablation rate at 125 kft.

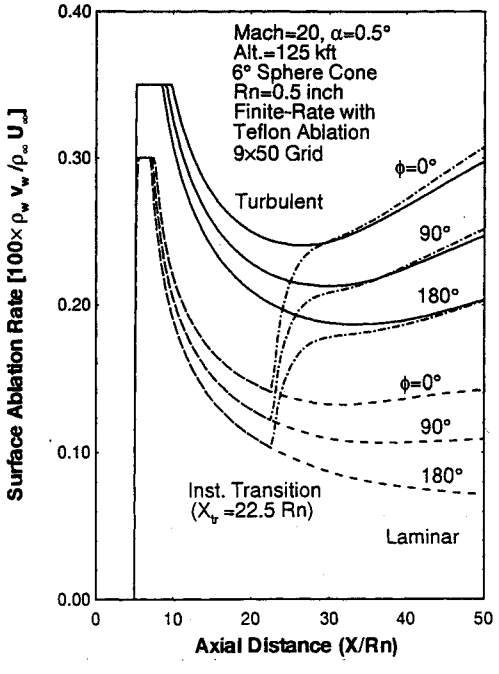

Fig. 3 Predicted ablation-rate distribution at 125 kft and $\alpha = 0$ deg.

Governing Equations

We chose our vector of flowfield unknowns to be

$$q = [\rho, \rho u, \rho v, \rho w, T, p]^T \tag{1}$$

Following the approach of Peyret and Viviand,[19] the three-dimensional Navier-Stokes equations are transformed into the general curvilinear coordinate system ξ_j. After neglecting the viscous dissipation effects in the ξ_1 direction and using the "thin-layer approximation" for small angles of attack to neglect the crossflow dissipation effects, we obtain the following vectorial form of the thin-layer PNS equations

$$f_{j,\xi_j} = \epsilon s_{2,\xi_2} + h \tag{2a}$$

where it is assumed that the freestream behaves as a perfect gas.

These five equations [Eqs. (2a)] representing the differential conservation of mass, momentum, and energy are mathematically closed by using the equation of state for the particular gas model being used. In the case of finite rate chemically reacting air, the gas is assumed to be a mixture of perfect gases and the equation of state is given by

$$p - \rho T/\bar{m} = 0 \tag{2b}$$

It should be noted that the energy equation for the present study is written in terms of the conservation of total enthalpy.

The mixture thermodynamic properties (such as $\bar{m}$, $\bar{k}$, $\bar{Cp}$, $\bar{\mu}$, Pr, Le, etc.) require a knowledge of the species concentrations C_i which are obtained from the species conservation equations.[1,20] These equations are first transformed to the curvilinear coordinate system ξ_j, and the resulting equations are parabolized by neglecting diffusion effects in the ξ_1 direction. Furthermore, the thin-layer approximation is also used to neglect the crossflow dissipation effects ($C_{i,\xi_3\xi_3} = 0$). The final thin-layer parabolized species conservation equations are written as

$$[(\rho U_j/J)C_i]_{,\xi_j} - \epsilon[(\bar{\mu} Le_i m_{2kk}/JPr)C_{i,\xi_2}]_{,\xi_2} = \dot{\omega}_i \tag{3}$$

where $i = 1, 2, 3, \ldots, NS$.

Numerical Solution Scheme

The system of equations represented by Eqs. (2) and (3) is closed through a knowledge of the thermodynamic and transport properties of the mixture; namely, $\bar{m}$, $\bar{k}$, $\bar{Cp}$, $\bar{\mu}$, Pr, and Le. For many practical problems, the coupling between the fluid mechanics (ρ, ρu, ρv, ρw, ρT, and p) and the chemistry ($\bar{Cp}$, $\bar{\mu}$, Pr, C_1, C_2, C_3, . . . , C_{NS}) is not very strong, and we can decouple the overall nonequilibrium PNS problem into 1) a fluid mechanics problem and 2) a chemistry problem.[1-7] During each iteration at a given marching step, we first solve the fluid-mechanics problem [Eqs. (2)], and then we solve the chemistry problem [Eqs. (3)] based on the solution to the fluid-mechanics problem. With this updated chemistry, the fluid-mechanics problem is solved once again, and the cycle is repeated until acceptable convergence is achieved.

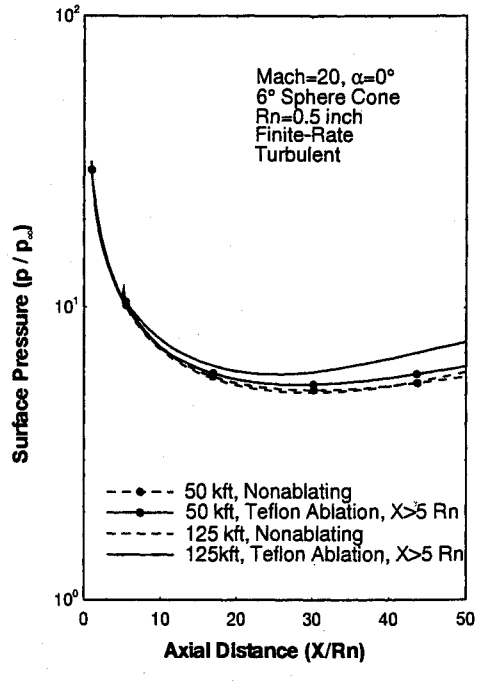

Fig. 4 Effects of surface ablation on the predicted surface-pressure distribution at $\alpha = 0$ deg.

Solution of the Fluid-Mechanics Problem

Except for the small angle-of-attack limitation, the solution scheme used for the fluid-mechanics problem is very similar to our approach of Refs. 1–7 and 13. With the small angle-of-attack assumption, we assume that the crossflow convective effects are small compared to the streamwise and axis-normal convective effects. This assumption is then used to simplify the numerical crossflow solution[3] by assuming that the crossflow convective terms at the $n + 1$ iteration can be approximated by its value at the previous iteration ($\tilde{f}_3^{n+1} \approx f_3^n$). In general, it is assumed that the solution at the $(n + 1)$ level is close to the solution at the nth iteration. Thus, after expanding the solution around the nth iteration, the flowfield equations are solved using a pseudounsteady approach,[1-7] fourth-order axis-normal and crossflow numerical diffusion effects,[1,13] second-order streamwise numerical dissipation effects,[1,13] and solution under-relaxation.[1,13]

Solution of the Chemistry Problem

In this study, the numerical approach used to solve the chemistry problem is based on our recently developed two-step coupled-chemistry scheme,[1] which was appropriately modified to include the crossflow convective effects in the element and species conservation equations.

Briefly stated, using the solution of the fluid-mechanics problem [Eqs. (2)], first the thermodynamic and transport properties of the reacting gas mixture are determined. This information is then used to solve the coupled-species equations, which are split into two user-specified groups of *NM* and *NE* species, where $NM + NE = NS - 1$. For simplicity, we refer to the group containing the *NE* species as group 1, and the group containing the *NM* species as group 2.[1] The coupled-species solution for the chemistry problem consists of the following main steps[1]:

1) Obtain the element mass fractions of all elements at each grid point using the element conservation equations.

2) Set up *NE* algebraic equations representing the conservation of elemental mass at each grid point.

3) Set up *NM* differential equations representing the conservation of mass of the *NM* species included in group 2.

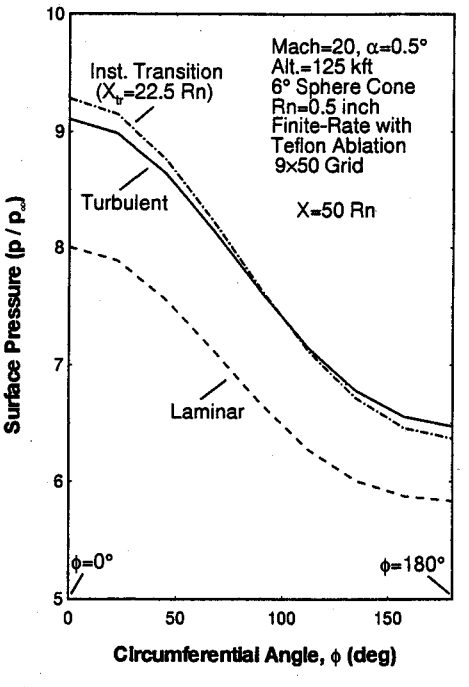

Fig. 5 Effects of surface ablation on the predicted crossflow surface-pressure distribution at $\alpha = 0.5$ deg.

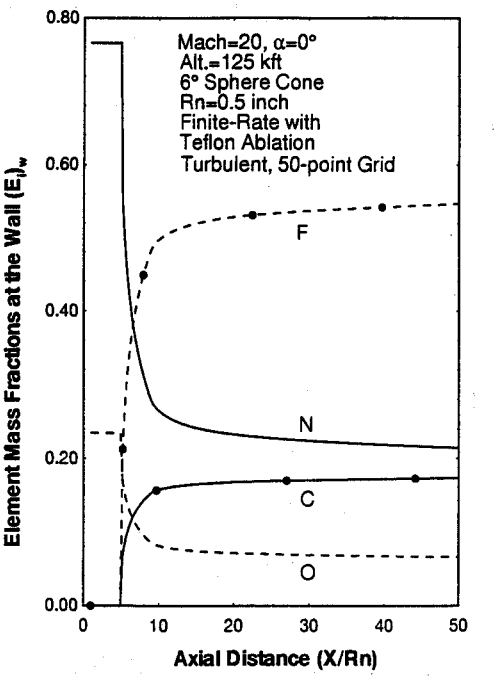

Fig. 6 Predicted element composition at the wall at 125 kft and $\alpha = 0$ deg.

4) Solve the $NE + NM$ equations simultaneously to obtain the species mass fractions at each grid point.

The final block-matrix system of equations representing the coupled-species conservation equations is solved using the two-step approach of Bhutta and Lewis.[1]

Boundary Conditions

The problem represented by the governing three-dimensional PNS equations is a split boundary-value problem. The initial conditions to start the present PNS scheme were obtained from compatible blunt-body viscous shock-layer (VSL) schemes,[21,22] and the shock boundary conditions were imposed using the implicit shock-fitting approach mentioned earlier.

In this study only a sphere-cone configuration was considered. For such axisymmetric bodies of revolution, the flowfield boundary conditions at the wall consist of 1) equation of state of the gas ($p - \rho T/m = 0$), 2) no-slip condition for u velocity component ($\rho u = 0$), 3) specified surface ablation rate in the y-coordinate direction ($\rho w = \dot{m} \sin \phi$), 4) specified surface ablation rate in the z-coordinate direction ($\rho w = \dot{m} \cos \phi$), 5) specified wall temperature [$(\rho T) = \rho T_w$], and 6) zero pressure derivative in the ξ_2 direction ($p_{,\xi_2} = 0$) where ϕ is the circumferential angle. The corresponding wall boundary conditions for the coupled-species conservation equations [Eqs. (3)] consist of either 1) fully catalytic wall boundary [$C_i = C_{i\infty}$] for the nonablating regions, or 2) equilibrium-catalytic wall boundary [$C_{iw} = C_i^{EQ}(\rho_w, T_w)$] for ablating regions where $i = 1, 2, \ldots, NS$.

Quasisteady Ablation Modeling of Teflon

Teflon (DuPont trade name) is a tetrafluoroethylene polymer that is widely used as a low-temperature ablator for re-entry applications. In this study, we have modeled Teflon surface-ablation effects with an accurate coupled-ablation model[1] which accounts for the different densities of Teflon in crystalline and amorphous states,[1] and is equally valid for laminar, transitional, and turbulent flow conditions.[1] After properly including all important modes of heat transfer to and

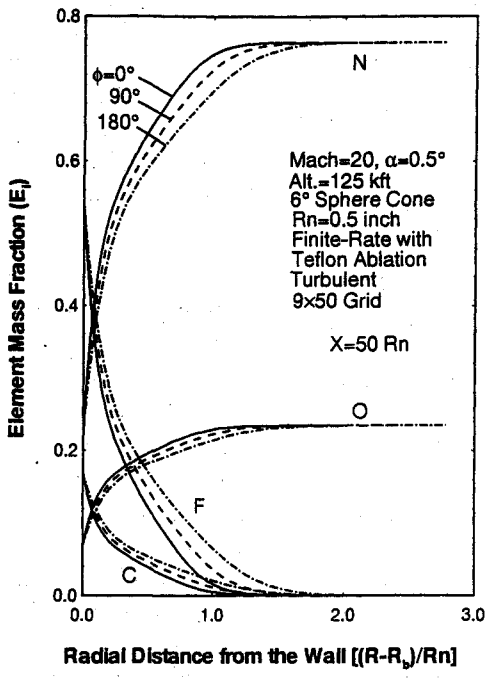

Fig. 7 Predicted element concentration profiles at 125 kft and $\alpha = 0.5$ deg.

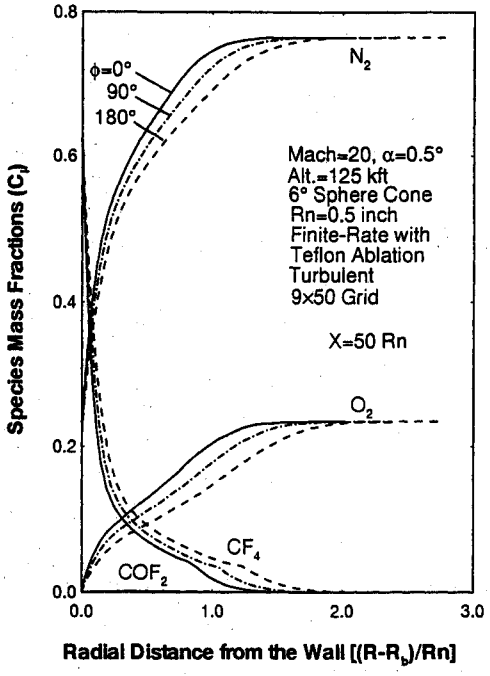

Fig. 8 Predicted concentration profiles of some dominant species at 125 kft and $\alpha = 0.5$ deg.

from the ablating surface, it can be shown[1] that the quasi-steady surface ablation rate $\dot{m}$ for Teflon is

$$\dot{m} = \frac{-(Q_c + Q_d)}{[h_w - (\rho_i/\rho_s)h_i]} \tag{4}$$

where h_w is the specific enthalpy of the gaseous mixture at the wall, and h_i is the specific enthalpy of the in-depth solid Teflon.[1] In Ref. 1 we have developed an accurate way of estimating this in-depth enthalpy by using the gaseous wall enthalpy as the reference, and interested readers are referred to that work for additional details.

Results and Discussion

To study the three-dimensional effects of ablation under laminar/transitional/turbulent flow conditions, several calculations were done using a 6-deg sphere-cone configuration with a nose radius of 0.041667 ft (0.5 in.). Since the present study was primarily intended to be an extrapolation of the coupled transition and ablation effects, effects of body length were not investigated, and the length of the test configuration was chosen to be $50Rn$ to reduce computing time requirements. The freestream Mach number was kept fixed at 20, and two different altitudes were tested: 50 and 125 kft. The freestream conditions corresponding to these altitudes are given in Table 1. Zero angle-of-attack studies were done at both 50 and 125 kft altitude, whereas 0.5-deg angle-of-attack calculations were only done at 125 kft. Furthermore, the 50-kft ablation calculations were done using a fully turbulent flow condition, whereas the 125-kft calculations were done using laminar/transition/turbulent flow conditions.

The computational grids used for these calculations consisted of 1-plane 100-point solutions at the lower (50 kft) altitude where the boundary layer is much thinner, and 1-plane and 9-plane solutions at the upper altitude (125 kft) with 50 points between the body and the shock. The 9-crossflow-plane solution was adequate for these angle-of-attack calculations, because the angle of attack considered was small (0.5 deg). For the 50- and 100-point grid, the grid spacing at the wall was 1×10^{-2} of the local shock standoff distance.

The following sections summarize some of the important results of these calculations. Unless otherwise noted, the wall temperature for these calculations was kept constant at 1800°R, and the sodium contamination at the wall was assumed to be 150 ppm. For all cases the blunt-body starting solutions were obtained from an equilibrium-air VSL scheme.[22] At 50 kft the flow across the bow shock was assumed to be in equilibrium, whereas a frozen shock was assumed for the 125 kft cases. For all of the cases with surface ablation, the forebody region up to $x = 5Rn$ was assumed to be nonablating, and ablation was abruptly started at $x = 5Rn$. Typically, when ablation was turned on instantaneously, the species concentrations at the wall suddenly became nonzero and, thus, showed unrealistically large gradients which increased the diffusion heat transfer to the wall. Consequently, the predicted ablation rates in this onset-of-ablation region was generally much too large and could cause a numerical blow off of the viscous layer. Thus, to prevent this nonphysical situation, the predicted ablation rate in the onset-of-ablation region was limited to some reasonable maximum value. Generally, this region was a few nose radii long and, thus, did not affect the overall predictions.

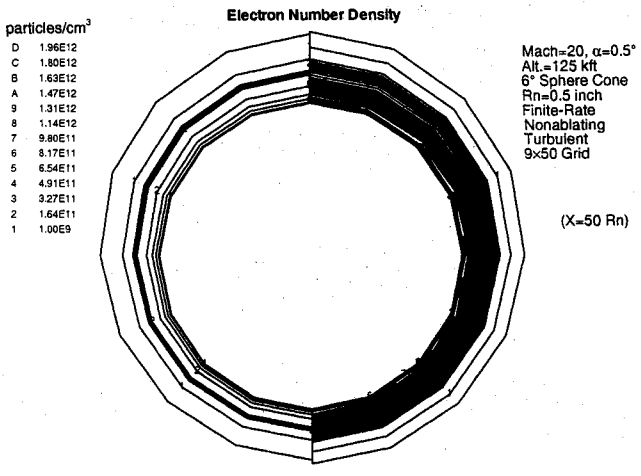

Fig. 9 Predicted electron density contours for turbulent flow at 125 kft and $\alpha = 0.5$ deg with and without ablation.

Teflon Surface-Ablation Rate Predictions

The turbulent predictions of the surface-ablation rate at 50 kft are shown in Fig. 1. In this figure the results of the empirical correlation of Brewer[23] for turbulent flows is also shown. As can be seen, the predictions of the correlation are approximately 30% higher; however, considering the empirical nature of the correlation, this comparison is still very good. We used Brewer's correlation with the no-blowing, turbulent heat transfer predictions of our perfect-gas PNS scheme.[13,14] It is interesting to note that Brewer's correlation was simply a refitting of available recession-history data to adjust for inaccuracies in the associated heat-transfer predictions, and essentially resulted in lower ablation-rate predictions.

The zero angle-of-attack laminar, transitional, and turbulent predictions of the surface-ablation rates at 125 kft are shown in Fig. 2. In this case comparisons are also made with the laminar correlation of Scala[24] and Brant.[25] The present laminar ablation-rate predictions are in excellent agreement with the laminar correlation of Scala. The turbulent ablation-rate estimates using Brewer's correlation[23] are again approximately 40% higher. In this case, the transitional flow calculations were done using the Dhawan-Narasimha transition model,[26] and transition was initiated at $x = 22.5Rn$. The results show that the transitional ablation-rate predictions smoothly change from the laminar ablation rates to the fully turbulent levels. It is interesting to note that existing approaches for estimating ablation rates are based on use of the available correlations,[23-25] which are either for fully turbulent or fully laminar flow conditions. The present approach represents the first known consistent and accurate prediction of the expected ablation rates in the transition region.

The surface-ablation-rate predictions for the laminar, transitional, and turbulent calculations at 125 kft with 0.5-deg angle of attack are shown in Fig. 3, and show the predictions along the windward, side, and leeward planes. For the transitional calculations shown in Fig. 3, the flow was instantaneously transitioned to fully turbulent conditions at $x = 22.5Rn$. In general, the predicted ablation rates are smooth and well behaved. Interestingly, the predicted windward ablation rate at the body with instantaneous transition at $x = 22.5Rn$ is about 5% higher than the corresponding fully turbulent predictions, suggesting that location of transition does have some effect on the surface-ablation rate. The subsequent results will demonstrate this coupling effect in more detail.

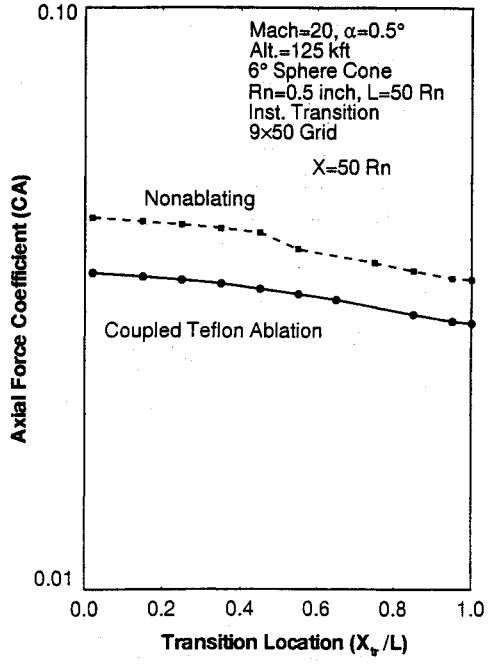

Fig. 10 Effects of transition and ablation on the axial force.

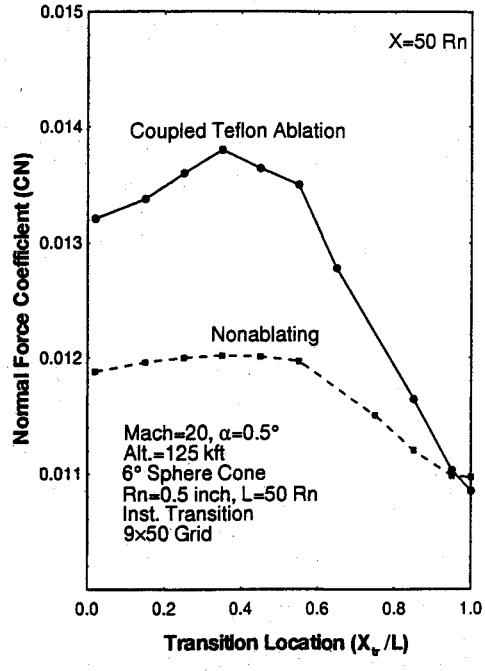

Fig. 11 Effects of transition and ablation on the normal force.

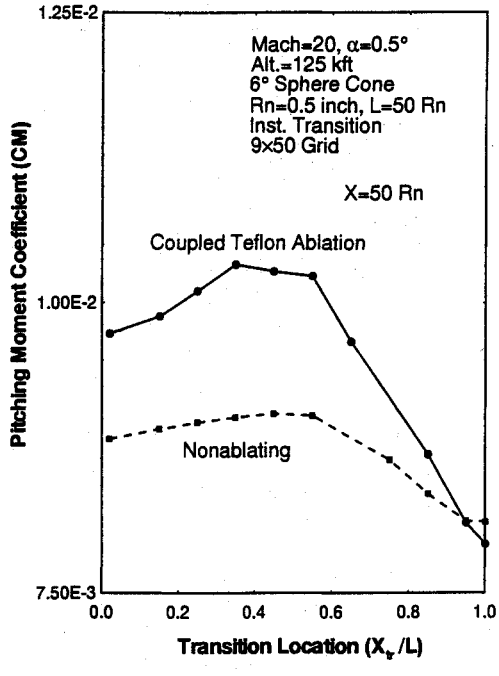

Fig. 12 Effects of transition and ablation on the pitching moment.

The effect of wall temperature on the ablation modeling and the predicted ablation rates was tested at 50 kft using 1800 and 2100°R wall temperatures. The results obtained showed that increasing the wall temperature from 1800 to 2100°R decreased the prediction ablation rates by approximately 10%. Thus, although there is some effect of the wall temperature, it is not large, and the assumption of a constant wall temperature of 1800°R is adequate for these studies.

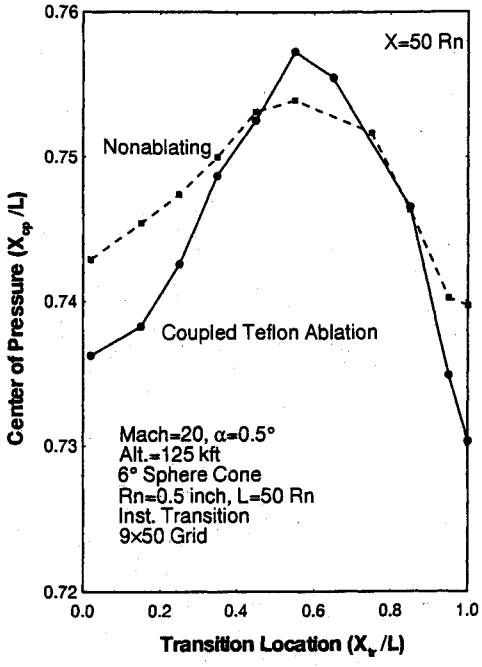

Fig. 13 Effects of transition and ablation on the center of pressure.

Effects of Surface Ablation on Surface Pressure

The effects of surface ablation on the predicted wall pressure distribution are shown in Figs. 4 and 5. The axial distributions of wall pressure at 50 and 125 kft under zero angle-of-attack conditions are shown in Fig. 4, which also shows the wall pressure prediction for the corresponding nonablating conditions. These results show that, at both 50- and 125-kft altitudes, surface ablation does result in noticeable viscous induced pressure. This increase in surface pressure becomes larger with increasing altitude. At 50 kft, surface ablation causes the surface pressure to increase by approximately 10%, whereas at 125 kft this increase is as much as 30%. The crossflow surface-pressure distributions at 125 kft for the 0.5-deg angle of attack are shown in Fig. 5. These results show that, compared to the laminar ablating conditions, the combined effects of transition/turbulence and ablation increase the surface pressure by as much as 15%. Interestingly, with instantaneous transition occurring at $x = 22.5Rn$, the increase in the windward surface pressure is more than the fully turbulent case, whereas the increase in the leeward surface pressure is less. Thus, we see that the combined effects of transition and ablation can affect the windward and leeward surface pressures resulting in additional normal-force and pitching-moment effects. Furthermore, the large difference between the laminar and turbulent predictions suggest that effects such as asymmetric transition front and different transition lengths on the windward and leeward sides can further enhance these effects and may give rise to even larger changes in the pitching moment and normal force.

Effects of Surface Ablation on Flowfield Chemistry

The predicted element compositions at the wall for zero angle-of-attack calculations at 125-kft altitude are shown in Fig. 6. These results show that, with the proper convection-diffusion wall boundary condition for the element conservation equations,[1] the ablation elements (C, F, and Na) show a gradual buildup in the streamwise direction and then asymptote to some value which is less than 1. This buildup of the concentration of ablation elements at the wall is slightly quicker and larger at 50 kft than at 125 kft. These results show that ablation techniques which assume the species composition at the wall to be purely ablation elements[14] are not correct.

The body-end, turbulent concentration profiles of important elements and species at 0.5-deg angle-of-attack case and 125 kft are shown in Figs. 7 and 8 and show that significant effects of surface ablation extend through approximately 50% of the shock layer. The corresponding electron number-density contours at the body end with and without ablation are compared in Fig. 9. These figures show that, with Teflon surface ablation, the electron number densities in the near-wall region are several orders of magnitude larger. In fact, with ablation, almost 50% of the shock layer shows considerably higher concentrations of electrons.

Effects of Transition and Ablation on Force and Moment Predictions

The effects of coupled transition and ablation at 0.5-deg angle of attack and 125 kft were studied using 10 different transition locations ranging from fully laminar ($x_{tr}/L = 1$) to fully turbulent ($x_{tr}/L = 0$) conditions. All of these transition calculations were done using an instantaneous transition to turbulence at the transition location. Corresponding nonequilibrium calculations were also done using a nonablating wall to isolate the effects of ablation. Figure 10 shows the effects on the axial-force coefficient CA, which decreases with surface ablation by approximately 20% and increases by approximately 10% as the transition front moves over the body. The normal-force coefficient CN and the pitching-moment coefficient CM variations are shown in Figs. 11 and 12. These results show that as the transition front moves upstream over the body (flow changes from laminar to fully turbulent), the normal force and pitching moment of the body increases and then decreases. As shown earlier in Fig. 5, the combined effect of transition and ablation is to introduce asymmetries in the flow which give rise to larger normal force and pitching mo-

Table 2 Computing times for cases 1-3

Case	Alt, kft	M_∞	AOA,[a] deg	Flow type[b]	MDOT[c]	Grid,[d] $N3 \times N2 \times N1$	Time,[e] min:s
1a	50	20	0	Trb	=0	1 × 100 × 114	1:36
1b	50	20	0	Trb	>0	1 × 100 × 117	2:41
2a	125	20	0	Trb	=0	1 × 50 × 140	1:13
2b	125	20	0	Trb	>0	1 × 50 × 140	1:40
2c	125	20	0	Lam	>0	1 × 50 × 140	1:50
3a	125	20	0.5	Trb	=0	9 × 50 × 142	7:10
3b	125	20	0.5	Trb	>0	9 × 50 × 142	10:32
3c	125	20	0.5	Lam	>0	9 × 50 × 142	11:26

[a]AOA = angle of attack.
[b]Trb = turbulent, Lam = laminar.
[c]MDOT = 0 means nonablating, whereas MDOT > 0 means coupled Teflon ablation for $x > 5Rn$.
[d]$N1$, $N2$, and $N3$ are the number of grid points in the streamwise, axis-normal, and crossflow directions, respectively.
[e]Computing times on Cray Y-MP with CFT77 compiler and autovectorization.

ment. These asymmetries decrease as the flow becomes fully turbulent and, thus, the normal force and pitching moment experienced by the body also decrease.

The corresponding variations in the center-of-pressure location are shown in Fig. 13, and show that for both ablating and nonablating cases the center of pressure initially increases as the flow becomes transitional and then decreases as the flow becomes fully turbulent. However, with surface ablation, the difference between the maximum and minimum center-of-pressure location is much larger and changes by as much as 3%. From a guidance and vehicle aerodynamics point of view, these are significant changes in the center of pressure and cannot be ignored. Clearly, additional asymmetric features such as asymmetric transition and asymmetric transitions lengths can significantly increase these variations in the center of pressure.

Computing Times

The computing times for some of the zero and nonzero angle-of-attack cases with and without ablation are shown in Table 2 along with the grids used for these calculations. In general the various angle-of-attack ablation calculations done in this study took between 7 and 12 min each on the Cray Y-MP. It should be noted that the code used for these calculations is a research code, and thus no special efforts were made to minimize the computing times. Even so, considering the complexity and size of the ablation problem, the computing times are quite reasonable.

Conclusions

A new coupled-chemistry PNS scheme has been developed to study three-dimensional hypersonic re-entry flows over sphere cones at small angles of attack. A new quasisteady ablation model for Teflon was used to predict ablative re-entry flowfields under laminar, transitional, and turbulent conditions. This three-dimensional coupled-chemistry solution scheme uses a new two-step solution scheme for solving the species conservation equations under low-altitude conditions and was used to study hypersonic flow over a 6-deg sphere-cone configuration at 50- and 125-kft conditions under zero and small angle-of-attack conditions. The results of these studies substantiate the following comments.

1) The two-step solution scheme developed by Bhutta and Lewis[1] is quite stable and accurate and represents a computationally efficient way of predicting low-altitude ablative re-entry flows.

2) The quasisteady Teflon ablation model of Bhutta and Lewis[1] is equally valid under laminar, transitional, and turbulent conditions. Comparisons with existing empirical correlations for Teflon ablation show that the agreement with Scala's[24] and Brant's[25] laminar correlation is very good, but Brewer's turbulent correlation[23] overpredicts the ablation rate by as much as 40%.

3) Teflon surface ablation has significant effects on the surface pressure distribution. Furthermore, compared to laminar conditions, the coupled effects of turbulence and ablation can increase the surface pressure by as much as 30%.

4) The combined effects of transition and ablation introduce significant asymmetries in the flow and, thus, give rise to a larger normal force and pitching moment.

5) As the transition front moves over the re-entry body, the combined effects of transition and ablation can significantly change the vehicle's center of pressure. For the conditions tested, the change in the center-of-pressure location was as much as 3%.

6) The results of this study indicate that a reliable, accurate, and efficient nonequilibrium PNS afterbody scheme has been developed to predict the hypersonic re-entry flowfields over BRV/MaRV/decoy configurations with complex chemistry at small angles of attack and with surface ablation effects over a wide range of altitudes. This small-angle-of-attack scheme can be readily extended to large-angle-of-attack flows and other chemical systems.

Acknowledgments

The work reported in this paper was supported in part by the NASA Lewis Research Center under Contract NAS3-25450. The encouragement and cooperation provided by Louis Povinelli, Dan Whipple, Allan Bishop, and the contract monitor Tom Benson during the course of this effort are gratefully acknowledged. The authors would also like to thank James Daywitt and Darius N. Brant of General Electric Re-entry Systems Department, Philadelphia, Pennsylvania, for their valuable suggestions about Teflon ablation modeling, and their help in obtaining the correlations for Teflon ablation.

References

[1]Bhutta, B. A., and Lewis, C. H., "New Technique for Low-to-High Altitude Predictions of Ablative Hypersonic Flowfields," *Journal of Spacecraft and Rockets,* Vol. 29, No. 1, 1992, pp. 35–50; see also AIAA Paper 91-1392, June 1992.

[2]Bhutta, B. A., and Lewis, C. H., "Low Reynolds Number Flows Past Complex Multiconic Geometries," AIAA Paper 85-0362, Jan. 1985.

[3]Bhutta, B. A., Lewis, C. H., and Kautz, F. A., II, "A Fast Fully-Iterative Parabolized Navier-Stokes Scheme for Chemically-Reacting Re-Entry Flows," AIAA Paper 85-0926, June 1985.

[4]Bhutta, B. A., and Lewis, C. H., "Three-Dimensional Hypersonic Nonequilibrium Flows at Large Angles of Attack," *Journal of Spacecraft and Rockets,* Vol. 26, No. 3, 1989, pp. 158–166; see also AIAA Paper 88-2568, June 1988.

[5]Bhutta, B. A., and Lewis, C. H., "Prediction of Nonequilibrium Viscous Hypersonic Flows Over Lifting Configurations," AIAA Paper 89-1696, June 1989.

[6]Bhutta, B. A., and Lewis, C. H., "Three-Dimensional Parabolized Navier-Stokes Predictions of Hypersonic Nonequilibrium Flows Over Ablating Teflon Surfaces; Volume I: Technical Report; Volume II: User's Manual," VRA, Inc., VRA-TR-87-02, Blacksburg, VA, Dec. 1987.

[7]Bhutta, B. A., Song, D. J., and Lewis, C. H., "Nonequilibrium Viscous Hypersonic Flows Over Ablating Teflon Surfaces," *Journal of Spacecraft and Rockets,* Vol. 27, No. 2, 1990, pp. 205–215; see also AIAA Paper 89-0314, Jan. 1989.

[8]Bhutta, B. A., and Lewis, C. H., "An Implicit Parabolized Navier-Stokes Scheme for High Altitude Re-Entry Flows," AIAA Paper 85-0036, Jan. 1985.

[9]Bhutta, B. A., and Lewis, C. H., "PNS Predictions of Three-Dimensional Hypersonic Flows with Strong Crossflow Effects," *Journal of Thermophysics and Heat Transfer,* Vol. 4, No. 1, 1990, pp. 27–36; see also AIAA Paper 88-2696, June 1988.

[10]Bhutta, B. A., and Lewis, C. H., "Prediction of Three-Dimensional Hypersonic Flows using a Parabolized Navier-Stokes Scheme," *Journal of Spacecraft and Rockets,* Vol. 26, No. 1, 1989, pp. 4–13; see also AIAA Paper 85-1604, July 1985.

[11]Bhutta, B. A., and Lewis, C. H., "Prediction of Axisymmetric Hypersonic Blunt-Body Flows Using a Parabolized Navier-Stokes Scheme," AIAA Paper 89-1831, June 1989.

[12]Bhutta, B. A., and Lewis, C. H., "Comparison of Hypersonic Experiments and PNS Predictions Part I: Aerothermodynamics," *Journal of Spacecraft and Rockets,* Vol. 28, No. 4, 1991, pp. 376–386; see also AIAA Paper 90-3068, Aug. 1990.

[13]Bhutta, B. A., and Lewis, C. H., "Comparison of Hypersonic Experiments and PNS Predictions Part II: Aerodynamics," *Journal of Spacecraft and Rockets,* Vol. 28, No. 4, 1991, pp. 387–393; see also AIAA Paper 90-3068, Aug. 1990.

[14]Finson, M. L., Ameer, P. G., Person, J. C., Cronin, J. F., and Parker, P. D., "Non-Equilibrium Boundary-Layer Code; Volume I of II, Numerical Methodology; Volume II of II, User's Manual," Physical Sciences Inc., PSI-9030/TR-676, Andover, MA, June 1988.

[15]Widhopf, G. F., and Victoria, K. J., "On the Solution of the Unsteady Navier-Stokes Equations Including Multicomponent Finite Rate Chemistry," *Computers and Fluids,* Vol. 1, June 1973, pp. 159–184.

[16]Finson, M. L., and Ameer, P. G., "Non-Equilibrium Boundary-Layer Code," Physical Sciences Inc., PSI-069/TR-512, Andover, MA, May 1985.

[17]Li, C. P., "Implicit Methods for Computing Chemically Reacting Flow," NASA TM 58274, Sept. 1986.

[18]Blottner, F. G., Johnson, M., and Ellis, M., "Chemically Reacting Viscous Flow Program for Multi-Component Gas Mixtures," Sandia Laboratories, Rept. SC-RR-70-754, Albuquerque, NM, Dec. 1971.

[19]Peyert, R., and Viviand, H., "Computations of Viscous Compressible Flows Based on the Navier-Stokes Equations," AGARD-AG-212, 1975.

[20]Bird, R. B., Stewart, W. E., and Lightfoot, E. N., *Transport Phenomena,* Wiley, New York, 1960.

[21]Swaminathan, S., Kim, M. D., and Lewis, C. H., "Three-Dimensional Nonequilibrium Viscous Shock-Layer Flows over Complex Geometries," *AIAA Journal,* Vol. 22, No. 6, 1984, pp. 754–755; see also AIAA Paper 83-0212, Jan. 1983.

[22]Thareja, R. R., Szema, K. Y., and Lewis, C. H., "Chemical Equilibrium Laminar or Turbulent Three-Dimensional Viscous Flows," *Journal of Spacecraft and Rockets,* Vol. 20, No. 5, 1983, pp. 454–460; see also AIAA Paper 82-0305, Jan. 1982.

[23]Brewer, R. A., "Ablation Modeling of Teflon," General Electric Co., GE-RESD PIR-U-Y4-83-8T20-058, Philadelphia, PA, July 1983.

[24]Scala, S. M., "A Study of Hypersonic Ablation," General Electric Co., GE-RESD TIS-R59SD438, Philadelphia, PA, Sept. 1959.

[25]Brant, D. N., "Investigation of Teflon Performance on the MK 12 Nosetip," General Electric Co., GE-RESD PIR-9151-AE-104, Philadelphia, PA, Dec. 1973.

[26]Dhawan, S., and Narasimha, R., "Some Properties of Boundary Layer Flow During the Transition from Laminar to Turbulent Motion," *Journal of Fluid Mechanics,* Vol. 3, Jan. 1958, pp. 418–436.

Michael E. Tauber
Associate Editor